Built-In Test of MEMS Capacitive Accelerometers for Field Failures and Aging Degradation

Álvaro Gómez-Pau, Ricard Sanahuja, Luz Balado, Joan Figueras

Departament d'Enginyeria Electrònica, Universitat Politècnica de Catalunya
Av. Diagonal 647, 9th floor, E-08028 Barcelona (Spain)
{alvaro.gomez-pau, ricard.sanahuja, luz.m.balado, joan.figueras}@upc.edu

***Abstract*—Accelerometers to be used in safety critical applications require efficient testing and monitoring techniques in order to guarantee their on-field reliability. Device degradation due to aging is becoming a major concern because of its capabilities to cause parametric deviations and catastrophic failures in the mechanical and structural subsystems. In this work, a built-in test strategy is presented. It is based on the periodic observation of the output signal using the device self-test facility as excitation. Acceptance bounds are established for the output voltage according to 6σ specifications in addition to the self calibration of the device since the input self-test excitation varies significantly from device to device. Simulations carried out using a commercial Analog Devices ADXL series model under realistic scenarios show encouraging results in the detection of aging deviations under different structural and mechanical parameter degradations.**

***Index Terms*—Built-In Test, Accelerometer Test, Accelerometer Aging.**

I. Introduction

The International Technology Roadmap for Semiconductors 2011 establishes integration, packaging and test as the greatest challenges in current microelectromechanical systems. Testing and on-line failure monitoring of MEMS devices is complex, requires sophisticated approaches and entails various challenges beyond those found in classical VLSI circuits [1].

MEMS integrated devices to be used in safety critical applications demand novel test strategies and on-line degradation monitoring techniques to achieve allowable production yields and reliable devices. Failures of MEMS structures have been studied for different architectures and materials [2]–[4]. For sensors embedded in CMOS processes, the reliability and response of silicon and polysilicon is well known due to its use in classical IC fabrication processes. Basic failure mechanisms mainly include stiction, fatigue, moisture contamination, process variations, electrostatic discharges and material aging degradations [5]–[7]. These mechanisms can become catastrophic or parametric defects that need to be tested and monitored efficiently [8], [9].

In the case of MEMS accelerometers, some solutions have been proposed in the past as DFT and BIST techniques [10], [11]. There is a commercial digital test pin solution implemented in Analog Devices accelerometers [12], [13]. Commanded with a digital pin, an electrostatic force over specific outer combs mimics the inertial action of an acceleration force. The test pin allows functional and sensitivity validation online, but due to the process variability, every device needs to be laser trimmed as part of production calibration [14]. Some other research proposals use similar outer comb actuators commanded with analog signals to evaluate different sensor parameters for capacitive and thermal devices [15], [16].

Other proposals use electrical or physical stimulus that can be correlated with the parameters to be measured. In this way regression techniques can be used to predict or diagnose the behavior of the device. A digital LFSR generated signal is used in [17] and [18] to obtain the input/output transfer function from the impulse response of the device. In a similar way a code modulated sine wave with pseudorandom characteristics is added to the bias of an accelerometer [15] and correlation algorithms are evaluated to make a test decision. In [19] the *alternate test* approach used for mixed-signal circuits is applied to an accelerometer using multitone inputs and correlating the device parameters after circuit exercising. In [20] the authors use the test signal of a commercial accelerometer demonstrating the correlation between the input signal and the output response of the device. In [21], [22], the authors employ Lissajous compositions to test and diagnose faulty accelerometer devices.

In this paper we propose a built-in structure to periodically monitor the output voltage and make a test decision. Based on the self-test capabilities of ADXL series accelerometers, the output is compared against a set of reference levels in order to quantify the reliability hazard of the device. The paper is organized as follows. In section II basic MEMS accelerometer considerations are discussed and the mechanical and transducer subsystems models are introduced. Section III explains the different aging problems MEMS accelerometers suffer from and how they can be modeled. Section IV is devoted to show the way to observe several damages in MEMS accelerometers using the self-test pin facility implemented in Analog Devices ADXL series. In section V, the proposed built-in test architecture is described while in section VI some preliminary simulation results are presented. Finally, section VII summarizes the work and concludes the paper.

II. MEMS Capacitive Accelerometers

MEMS capacitive accelerometers are built as a chain of three functional blocks, namely: mechanical system, transducer and electronic conditioning (see Fig. 1). In this work, special emphasis is devoted to the mechanical and capacitive

transducer subsystems since they are more prone to present defects and be degraded by aging.

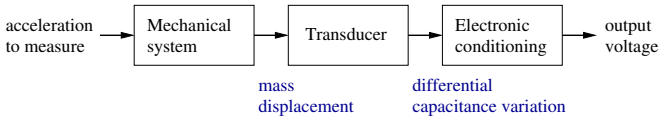

Fig. 1. Different stages of the acceleration transduction chain in MEMS capacitive accelerometers and the involved parameters.

In the following subsections, the models for the mechanical and transducer subsystems are presented and the typical self-test structure widely used in these types of accelerometers analyzed.

A. Mechanical System Model

The design and analysis of MEMS accelerometers dynamics is usually carried out by advanced ad-hoc methods and aided by computational strategies like the finite elements method (FEM) which is capable to provide accurate and realistic results.

The mechanics of inertial MEMS accelerometers can approximately be modeled in terms of three parameters, namely: the inertial mass, m, the damping factor, b, and the spring constant, k. Considering x to be the inertial mass displacement from its rest position and F_{ext} the external force applied to the system along the x axis, the following motion differential equation is satisfied, $m\ddot{x} + b\dot{x} + kx = F_{\text{ext}}$. As the external force is directly applied to the inertial mass, the equation to be considered is,

$$\ddot{x} + \frac{b}{m}\dot{x} + \frac{k}{m}x = a_{\text{ext}} \tag{1}$$

Equation (1) governs the kinematics and dynamics of the sensing axis and can be explicitly be written in the s domain as,

$$\frac{x}{a_{\text{ext}}} = \frac{\frac{m}{k}}{\frac{m}{k}s^2 + \frac{b}{k}s + 1} \tag{2}$$

Transfer function (2) corresponds to a second order linear model of the inertial accelerometer mechanical system from which the critical angular pulsation frequency, ω_0, and quality factor, Q, can be directly identified,

$$\omega_0 = \sqrt{\frac{k}{m}}, \quad Q = \frac{\sqrt{km}}{b} \tag{3}$$

As a case example, ADXL203 [13] dual axis accelerometer presents the following parameters ratios, $m/k = 8.374 \times 10^{-10}$ s^2 and $b/k = 5.788 \times 10^{-6}$ s, which results in a critical frequency $f_0 = 5.5$ kHz and a quality factor $Q = 5$. Note that the ratio m/k is directly related to the DC response of the device and therefore to the accelerometer sensitivity specification.

B. Capacitive Transducer Structure Model

The sensor structure of MEMS capacitive accelerometers is a differential capacitor in which the varying parameter is the distance between plates. The sensor is composed of an inertial mass that is anchored to the fixed substrate structure by means of springs. The inertial mass has several comb fingers that interdigitate with another set of comb fingers in the fixed structure. These interdigitated fixed and movable combs form the differential capacitor structure as sketched in Fig. 2. Without any acceleration, the beam should be perfectly centered and both sides of the differential structure present the same capacitance value. When acceleration is present, the distance between plates increases in one side and shrinks the same amount in the other side, thus unbalancing the structure.

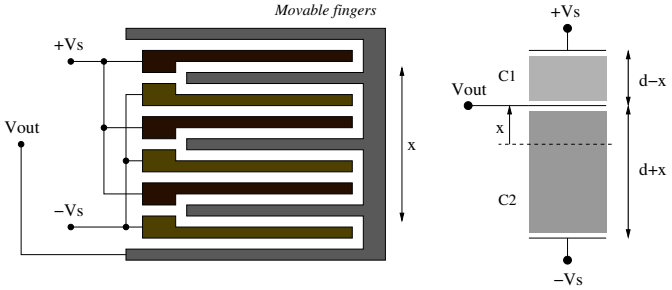

Fig. 2. Sketch of MEMS capacitive accelerometer transducer structure. Grey fingers can freely move along the x direction. The displacement unbalances the structure generating different C_1 and C_2 capacitances.

The transduction from acceleration to capacitance needs a capacitor measurement circuitry. The capacitance to voltage transduction can be accomplished in different ways. As an example, in commercial ADXL accelerometers the capacitor structure is supplied internally with an AC voltage that is modulated with capacitance variations. A stage of coherent demodulation to retain the sign, completes the conditioning to generate the analog output voltage [13]. Analog signal amplification, digital conversion and parallel or serial format outputs are added depending on the desired output characteristics of each device. Fig. 3 (left) shows a photography of the inertial mass architecture and anchors of a dual axis accelerometer composed of two identical orthogonally placed structures.

For low-g accelerometers the sensitivity needs to be precisely tuned, so the spring constant and the inertial mass are the parameters to be carefully designed as equation (8) indicates. By reducing the spring constant the sensitivity is improved but then the critical frequency falls within the range where the devices works. On the other hand, the inertial mass parameter directly affects the area of the device. As can be seen in Fig. 3 (right), dual low-g accelerometers may share the inertial mass thereby improving the sensitivity without an excessive device area increment [14]. The design in this case allows the XY plane movement of the mass and the spring system is designed to minimize the cross axis sensitivity.

If the capacitive structure depicted in Fig. 2 is fault-free and balanced with rest distance d between plates, plate area A and medium permittivity ε, both capacitances C_1 and C_2

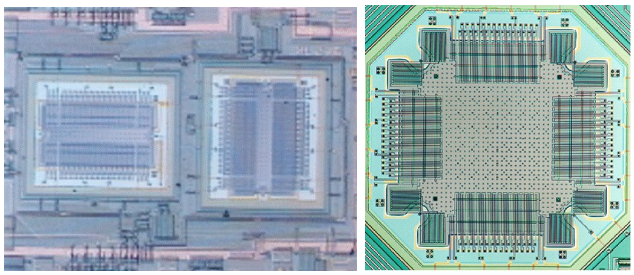

Fig. 3. Partial chip photography of ADXL250 dual axis accelerometer showing orthogonal sensor directions (left). Detail of ADXL202 dual axis accelerometer where the inertial mass is shared for both axes (right). Courtesy of Analog Devices.

are equal to $C_0 = \varepsilon A/d$. When an acceleration is applied, the structure unbalances to values,

$$\left.\begin{aligned} C_1 &= \frac{\varepsilon A}{d-x} = C_0 + \Delta C \\ C_2 &= \frac{\varepsilon A}{d+x} = C_0 - \Delta C \end{aligned}\right\} \tag{4}$$

The difference of capacitances C_1 and C_2 becomes,

$$C_1 - C_2 = \frac{\varepsilon A}{d-x} - \frac{\varepsilon A}{d+x} = 2\Delta C \tag{5}$$

From which the following second order equation is derived, $\Delta C x^2 + \varepsilon A x - \Delta C d^2 = 0$. If the displacement x is assumed to be small, the term $\Delta C x^2$ can be neglected and therefore solved for the mass displacement which shows to be approximately proportional to the unitary capacitance variation,

$$x \approx \frac{\Delta C d^2}{\varepsilon A} = \frac{\Delta C}{C_0}\, d \tag{6}$$

Regarding the output voltage of the capacitive voltage divider sketched in Fig. 2, it can be expressed in terms of mass displacement as,

$$V_{\text{out}} = \frac{\frac{\varepsilon_1 A_1}{d_1 - x} - \frac{\varepsilon_2 A_2}{d_2 + x}}{\frac{\varepsilon_1 A_1}{d_1 - x} + \frac{\varepsilon_2 A_2}{d_2 + x}}\, V_{\text{s}} \tag{7}$$

If no defects are present, $\varepsilon_1 A_1 = \varepsilon_2 A_2$ and $d_1 = d_2$, equation (7) simplifies to $V_{\text{out}} = x/d\, V_{\text{s}}$. Taking in consideration this result and the DC output response of the accelerometer when an aceleration a_{ext} is applied, its output voltage and sensitivity are,

$$V_{\text{out}} = V_{\text{offset}} + S\, a_{\text{ext}}, \quad S = \frac{m}{k}\frac{1}{d}\, G V_{\text{s}} \tag{8}$$

Where V_{s} is the supply voltage, V_{offset} is the offset voltage ($V_{\text{s}}/2$ in ADXL203 accelerometer), G is a generic gain, d is the rest distance between plates and m and k are the inertial mass and the spring constant.

III. On-Field Aging Degradation

MEMS devices are vulnerable to various failure mechanisms. Since most of MEMS devices contain movable parts, material fatigue and aging under long-term repeated cycling load may lead to potential device failures, which in turn degrades the device reliability. In the following subsections, the mechanical and structural subsystem degradation is analyzed.

A. Mechanical System

Accelerometers mechanical system aging degradation is mostly focused on the spring constant degradation. It can be shown that the spring constant parameter is proportional to Young's modulus. Consider a silicon rod of section S subjected to a force F. It is known that the applied mechanical stress should be proportional to the experimented unitary elongation, $F/S = E\,\Delta\ell/\ell_0$, being E the Young's modulus and $\Delta\ell/\ell_0$ the unitary elongation. If the terms of the previous equation are identified against Hooke's Law, the spring constant yields to be proportional to Young's modulus, $k = ES/\ell_0$.

The analytical fatigue degradation model presented in [7] corresponds to the following power law,

$$\frac{\Delta k}{k} = BN^b \tag{9}$$

The leasts squares fitting of the stiffness degradation curve of Fig. 4 yields parameters $B = -1.77 \times 10^{-8}$ and $b = 0.584$ which vary considerably from specimen to specimen.

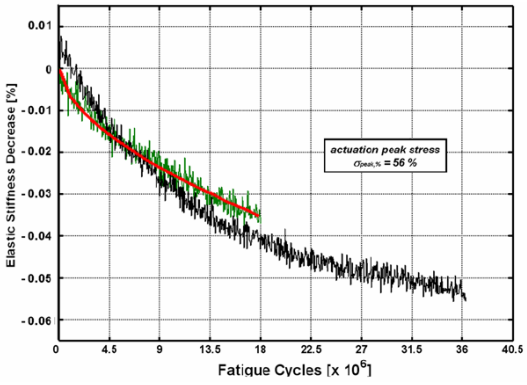

Fig. 4. Elastic stiffness degradation of polysilicon under fatigue conditions and the fitting (red trace) to a potential law of the form $\Delta k/k = AN^b$ [7].

Fatigue mechanisms in IC MEMS devices are an active area of research. Due to the small dimensions, grain orientations and crack propagation directions have a crucial role in early failures of such devices. Many studies are being conducted in order to characterize MEMS failure mechanisms [5], [6].

B. Capacitive Transducer Structure

Failures in the capacitive transducer structure are mainly due to changes in the capacitance of the structure. SiO_2 growth or medium permittivity contamination can degrade the

capacitive voltage divider presented in Fig. 2. In the subsequent sections, simulation experiments have been conducted assuming constant rate degradation of medium permittivities.

IV. Failures and Aging Degradation Observability in Output Voltage

Analog Devices ADXL series accelerometers implement a self test facility which is capable to electronically actuate over the inertial mass as if the IC was subjected to a physical acceleration. An experiment using a commercial device has been carried out. A 10 Hz square wave signal has been applied to its selft-test input and the output has been monitored. Fig. 5 shows the X axis selft-test response of ADXL203 when the mentioned wave is applied. The device exhibits a zero-g offset of 2.48 V when supplied with 5 V. The output signal amplitude is 0.72 V which corresponds to an excitation of 0.72 g assuming the nominal sensitivity of 1 V/g.

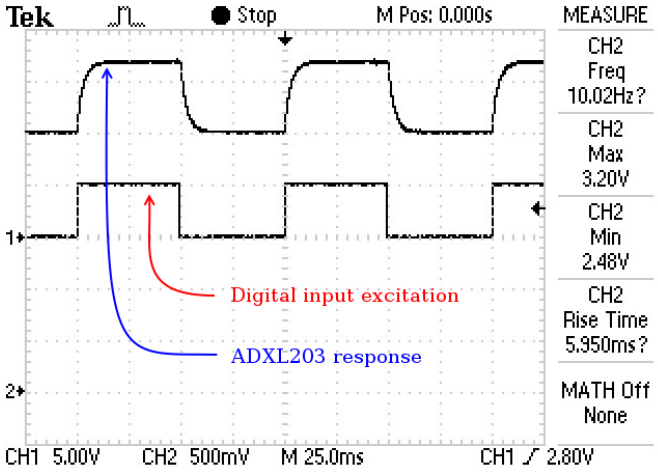

Fig. 5. Oscilloscope capture of the ADXL203 [13] output (X axis) when the self-test pin is excited with a digital signal. The output amplitude corresponds to 0.72 g of applied acceleration.

Data from ADXL203 datasheet [13] regarding the statistical distributions of the self-test applied acceleration and sensitivity. Fig. 6 shows the histograms of the mentioned parameters. As can be seen, the standard deviation of the self-test applied acceleration is 50 mg while the standard deviation of the sensitivity distribution is about 5 mV/g. This represents a factor of 10 and justifies the initial self-test calibration proposed and detailed in section V.

Deviations in the parameters of the mechanical system (inertial mass, spring constant) and transducer (medium permittivity, overlapping areas, rest distances between plates) subsystems are visible in the output voltage as they affect directly to the transduction chain (see expressions (2) and (7) and Fig. 1).

V. Proposed Built-In Architecture

As stated in previous sections, the self-test pin of Analog Devices ADXL series accelerometers can be used to easily test the device in the field. For this purpose, the architecture sketched in Fig. 7 is proposed.

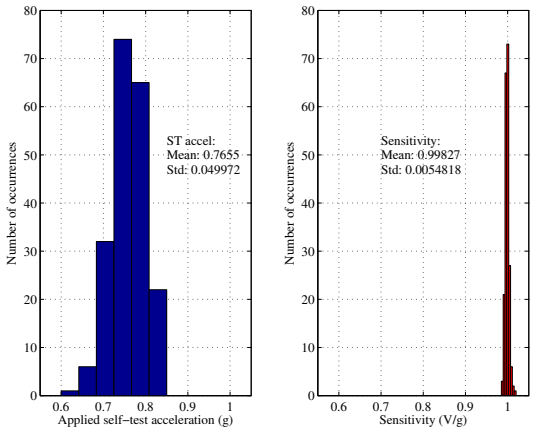

Fig. 6. Applied self-test acceleration (blue) and sensitivity (red) histograms of Analog Devices ADXL203 dual axis precision ± 1.7 g accelerometer [13]. Nominal self-test acceleration is 0.75 g with a standard deviation of 50 mg while nominal sensitivity is 1 V/g with a standard deviation of 5 mV/g.

The BIST architecture is formed by an analog to digital converter, a hysteresis level comparator and a controller.

Estimation of the mean value of V_{out}: Initially the device is tested and in case of passing the test, the initial value of the output voltage is converted to a digital 12-bits word and saved. Taking into account the variability band (sensitivity, electrical noise and temperature) provided by the manufacturer, the acceptance limits are computed by the controller. We denote this initial phase precalibration.

Field failures and aging degradation test: In order to detect possible changes due to aging or parametric variations causing reliability hazards or even failures, periodically, when the device is not active, the controller excites the self-test pin with a digital signal in order to electronically actuate over the inertial mass. The output voltage response of the device is digitized and compared against $\pm n\sigma$ ($n = 3, 4, 5$) specification levels by means of a digital hysteresis level comparator. The output of the BIST structure corresponds to one of the four reliability hazard severity levels detailed in Table I. The test result provides information about the conditions the device is working. For instance, a fresh and fault free device will report 00, as it is operating inside the $\pm 3\sigma$ specification bands. Under deep aging degradation or catastrophic failure, the output voltage will drop or rise beyond the $\pm 3\sigma$ limit. In this way, different reliability hazard severity levels will be identified so the controller will decide the appropiate action.

TABLE I
Reliability Hazard Severity Levels and their Codification

Level	Condition	Test output
1	Inside the $\pm 3\sigma$ band	00
2	Not in 1 but inside the $\pm 4\sigma$ band	01
3	Not in 2 but inside the $\pm 5\sigma$ band	10
4	Outside the $\pm 5\sigma$ band	11

According to Analog Devices ADXL203 ± 1.7 g accelerometer datasheet [13], the standard deviation for its sensitivity is $\sigma_S = 5$ mV/g which can be influenced by temperature according to a distribution with $\sigma_T = 3$ mV/g.

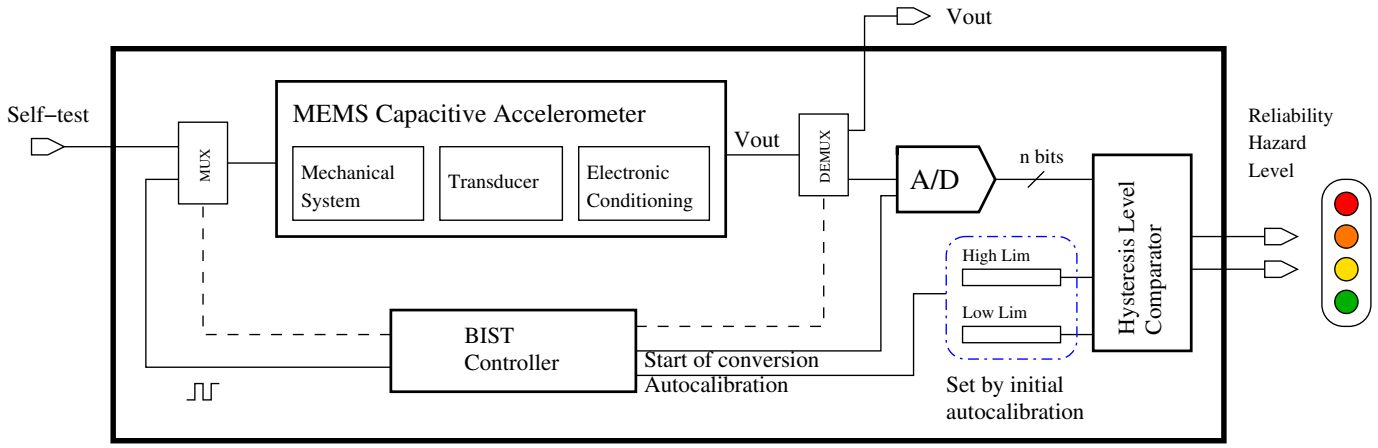

Fig. 7. Sketch of the proposed built-in self test architecture. Periodically, when the device is idle, the controller excites the self-test pin with a digital signal. The response is digitized and compared against reference levels which have been set in the initial autocalibration stage. The test result is one of the four possible reliability hazard severity levels codified using 2 bits as can be seen in Table I.

Finally, random noise standard deviation is estimated to be $\sigma_N = 3$ mV. Therefore, considering a nominal input acceleration of $a_{\text{nom}} = 0.75$ g, the overall standard deviation at the output yields to be,

$$\sigma = \sqrt{(a_{\text{nom}}\sigma_S)^2 + (a_{\text{nom}}\sigma_T)^2 + \sigma_N^2}, \quad \sigma = 6.1 \text{ mV} \quad (10)$$

Section IV described the considerable spread in the applied input acceleration when the self-test pin is excited as the histograms of Fig. 6 clearly shows. This means the self-test input excitation vary significantly from device to device. Because of this fact, an initial self calibration (precalibration phase) is required in order to remove the large variability reported by the manufacturer on the applied self-test acceleration.

VI. Simulation Experiments

In order to validate the proposal, simulation experiments have been carried out considering the BIST architecture presented in Fig. 7. MEMS capacitive accelerometer model described in section II has been used and simulated under realistic noise conditions. The noise levels have been assumed to be Gaussian with standard deviations specified in the previous section.

For illustration purposes and without loss of generality, the degradation scheme for the spring constant parameter is a constant degradation at a rate of -1%/year. Other values would present similar performances.

Fig. 8 shows the simulated output voltage for ADXL203 accelerometer considering the spring constant degradation pattern previously detailed. As expected, when decreasing the spring constant value, the ouput voltage increases because of their inverse proportionality as equation (8) states. At the very beginning of the simulation, the initial self-calibration is performed thereby allowing to establish the adequate $\pm n\sigma$ bands. The plot also shows each of the reliability hazard severity levels achieved when the spring constant starts to degrade.

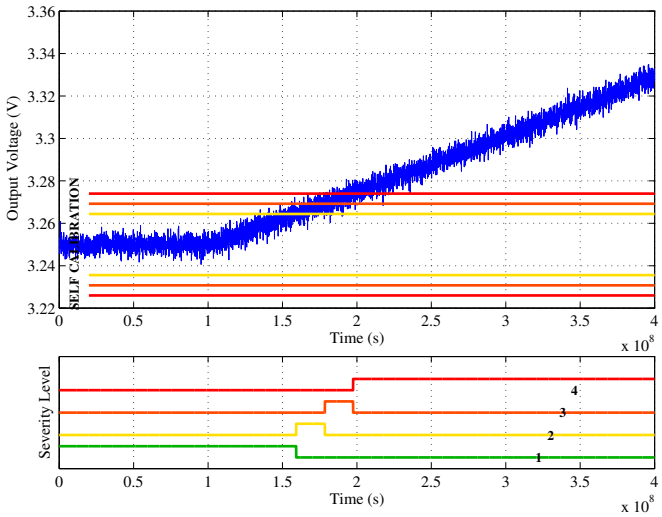

Fig. 8. Output voltage degradation due to a deviation in the spring constant, k, at a rate of -1%/year. The $\pm 3\sigma$, $\pm 4\sigma$ and $\pm 5\sigma$ bands as well as the four reliability hazard severity levels.

Similarly as performed for the spring constant, a degradation in the medium permittivities of capacitors C_1 and C_2 has been simulated. The resulting simulations of ADXL203 output voltage can be checked in figures 9 and 10. Again, a constant degradation of both permittivities has been assumed. Decreasing permittivity ε_1 makes the output voltage to decrease while decreasing permittivity ε_2 makes the output voltage to rise symmetrically.

VII. Conclusions

A built-in structure has been proposed for testing MEMS capacitive accelerometers. It is based on the periodic observation of the output voltage and check whether it lies within its acceptance band. The proposed architecture informs about the reliability hazard severity level depending on the output voltage value when it is excited using the self-test facility implemented by the manufacturers in such devices.

The proposed BIST architecture presents a low area over-

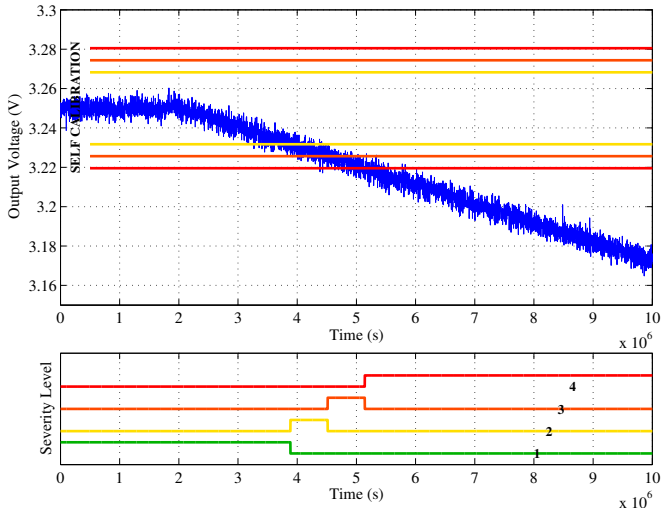

Fig. 9. Output voltage degradation due to a deviation in the medium permittivity, ε_1, of capacitor C_1, at a rate of -1%/year. The $\pm 3\sigma$, $\pm 4\sigma$ and $\pm 5\sigma$ bands as well as the four reliability hazard severity levels.

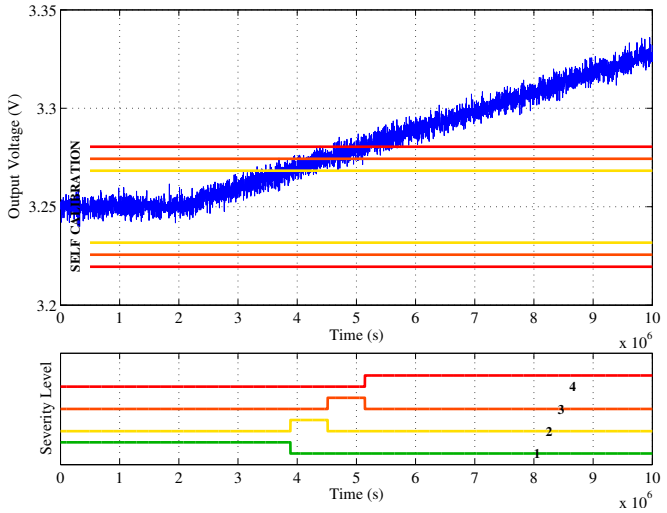

Fig. 10. Output voltage degradation due to a deviation in the medium permittivity, ε_2, of capacitor C_2, at a rate of -1%/year. The $\pm 3\sigma$, $\pm 4\sigma$ and $\pm 5\sigma$ bands as well as the four reliability hazard severity levels.

head compared with the integrated accelerometer structure since it only requires a digital controller, an analog to digital converter and a digital multi-level comparator that provides the two-bits test result information.

Realistic simulations conducted with typical internal noise of 3 mV show encouraging results in the detection of aging deviations under different structural and mechanical parameter degradations. The proposed BIST structure behaves as expected and reports the corresponding reliability hazard severity level according to the value of the output voltage when the device is not active and being tested.

ACKNOWLEDGMENTS

This work has been partially supported by the Spanish Ministry of Science and Innovation. Project reference is TEC2010-18384.

REFERENCES

[1] "International Technology Roadmap for Semiconductors," 2011, http://www.itrs.net/Links/2011ITRS/Home2011.htm.

[2] A. Kolpekwar, T. Jiang, and R. D. Blanton, "CARAMEL: Contamination And Reliability Analysis of Micro Electromechanical Layout," *Journal of Microelectromechanical Systems*, vol. 8, no. 3, pp. 309–318, 1999.

[3] N. Deb and R. D. Blanton, "Analysis of failure sources in surface-micromachined MEMS," in *Proceedings of the International Test Conference*, 2000, pp. 739–749.

[4] R. Rosing, A. Lechner, A. Richardson, and A. Dorey, "Fault simulation and modelling of microelectromechanical systems," *Computing and Control Engineering Journal*, vol. 11, no. 5, pp. 242–250, 2000.

[5] W. Sharpe Jr., B. Yuan, and R. Edwards, "A new technique for measuring the mechanical properties of thin films," *Journal of Microelectromechanical Systems*, vol. 6, no. 3, pp. 193–199, September 1997.

[6] B. Jalalahmadi, F. Sadeghi, and D. Peroulis, "A Numerical Fatigue Damage Model for Life Scatter of MEMS Devices," *Journal of Microelectromechanical Systems*, vol. 18, no. 5, pp. 1016–1031, October 2009.

[7] G. Langfelder, A. Longoni, F. Zaraga, A. Corigliano, A. Ghisi, and A. Merassi, "Real-time monitoring of the fatigue damage accumulation in polysilicon microstructures at different applied stresses," in *Proceedings of the IEEE Sensors Conference*, October 2009.

[8] A. Castillejo, D. Veychard, S. Mir, J. M. Karam, and B. Courtois, "Failure mechanisms and fault classes for CMOS-compatible microelectromechanical systems," in *Proceedings of the International Test Conference*, 1998, pp. 541–550.

[9] A. Soma and G. De Pasquale, "Reliability of MEMS: Effects of different stress conditions and mechanical fatigue failure detection," in *Proceedings of International Perspective Technologies and Methods in MEMS Design Conference (MEMSTECH)*, 2010, pp. 72–80.

[10] N. Deb and R. D. Blanton, "Multi-modal built-in self-test for symmetric microsystems," in *Proceedings of the 22nd VLSI Test Symposium*, May 2004.

[11] X. Xiong, Y. L. Wu, and W. B. Jone, "A dual mode built-in self-test technique for capacitive MEMs devices," *Transactions on Instrumentation and Measurement*, vol. 54, no. 5, pp. 1739–1750, October 2005.

[12] L. Zimmermann and et. al., "Airbag Application: a microsystem including a silicon capacitive accelerometer, CMOS switched capacitor electronics and true self-test capability," *Sensors and Actuators*, vol. 1, no. 3, pp. 190–195, January 1995.

[13] *ADXL203 dual axis accelerometer datasheet*, Analog Devices, 2010.

[14] H. Weinberg, "Dual Axis, Low g Fully Integrated Accelerometers," *Analogue Dialog*, vol. 33, no. 1, pp. 1–2, 1999.

[15] N. Dumas, F. Azaïs, F. Mailly, and P. Nouet, "Evaluation of a fully electrical test and calibration method for MEMS capacitive accelerometers," in *Proceedings of International Mixed-Signals, Sensors and Systems Test Workshop*, Vancouver, Canada, June 2008.

[16] A. A. Rekik, F. Azaïs, N. Dumas, F. Mailly, and P. Nouet, "An electrical test method for MEMs convective accelerometers: Development and evaluation," in *Proceedings of the Design Automation and Test in Europe Conference*, March 2011.

[17] L. Rufer, S. Mir, E. Simeu, and C. Domingues, "On-Chip Pseudo-random MEMS Testing," *Journal of Electronic Testing: Theory and Applications*, vol. 21, no. 3, pp. 233–241, June 2005.

[18] A. Dhayni, S. Mir, L. Rufer, and A. Bounceur, "Pseudorandom Functional BIST for Linear and Nonlinear MEMS," in *Proceedings of the Design, Automation and Test in Europe Conference*, 2006, July 2006, pp. 1–6.

[19] V. Natarajan, S. Bhattacharya, and A. Chatterjee, "Alternate Electrical Tests for Extracting Mechanical Parameters of MEMS Accelerometer Sensors," in *Proceedings of the VLSI Test Symposium*, April 2006.

[20] S. Dasnurkar and J. Abraham, "Characterization and testing of micro-electromechnical accelerometers," in *Proceedings of the 14th International Mixed-Signals, Sensors and Systems Test Workshop*, 2008, pp. 1–6.

[21] A. Gómez-Pau, L. Balado, and J. Figueras, "Testing IC Accelerometers Using Lissajous Compositions," in *Proceedings of International Perspective Technologies and Methods in MEMS Design Conference (MEMSTECH)*, Polyana, Ukraine, May 2011.

[22] A. Gómez-Pau, L. Balado, and J. Figueras, "Testing Dual Axis IC Accelerometers Using Lissajous Compositions," in *Proceedings of Design of Circuits and Integrated Systems Conference (DCIS)*, Albufeira, Portugal, November 2011.